Crossing fields in thin films of isotropic superconductors

V. K. Vlasko-Vlasov, F. Colauto, A. A. Buzdin, D. Carmo, A. M. H. Andrade, A. A. M. Oliveira,

W. A. Ortiz, D. Rosenmann, and W.-K. Kwok

Crossing fields in thin films of isotropic superconductors

V. K. Vlasko-Vlasov [1], F. Colauto[1,2], A. A. Buzdin[3], D. Carmo[2], A. M. H. Andrade[4],
A. A. M. Oliveira[5], W. A. Ortiz[2], D. Rosenmann[1], W.-K. Kwok[1]

[1] Argonne National Laboratory, 9700 South Cass Avenue, Argonne, Illinois 60439, USA
[2] Departamento de Fisica, Universidade Federal de Sao Carlos, 13565-905, Sao Carlos, SP, Brazil
[3] University Bordeaux, LOMA UMR- CNRS 5798, F-33405 Talence Cedex, France
[4] Instituto de Física, Universidade Federal do Rio Grande do Sul, 91501-970, Porto Alegre, RS, Brazil.
[5] Instituto Federal de Educacao, Ciência e Tecnologia de Sao Paulo, Campus Sao Carlos, 13565-905, Sao Carlos, SP, Brazil

We study interactions of perpendicular and longitudinal magnetic fields in niobium films of different thickness in a wide range of temperatures below the superconducting transition temperature (T_C). In 100 nm Nb film at all temperatures the longitudinal field $H_{||}$ practically does not influence the dynamics of the normal flux. However, in 200nm Nb film, a considerable anisotropy in the vortex motion is found with advanced propagation of the normal flux along $H_{||}$ at $T>T_C/2$ and the preferential jump-wise growth of the thermo-magnetic flux dendrites across $H_{||}$ at $T<T_C$. Appearance of the in-plane vortices and their cutting-reconnection with tilted vortices induced by the normal field $H_\perp$ is the reason of the observed anisotropy in the thicker film. Absence of the in-plane vortices and much smaller tilt of vortices generated by $H_\perp$ explain the isotropic normal flux dynamics in the thinner film. Our results open a new way of manipulating both slow vortex motion and fast thermo-magnetic avalanches.

Introduction

Despite a long history and substantial efforts to describe magnetic flux crossing in superconductors, the vortex cutting-reconnection phenomenon is still far from even qualitative clear comprehension (see [1] and refs there). Present work adds one more experimental evidence that the flux crossing brings a considerable effect on the vortex dynamics.

Recently, we investigated the normal magnetic flux ($B_\perp$) entry in a YBa$_2$Cu$_3$O$_{7-d}$ (YBCO) crystal plate magnetized with an in-plane field parallel to the superconducting CuO$_2$ layers ($H_{||}$) [2]. Direct flux imaging revealed pronounced anisotropic vortex dynamics with preferential vortex motion along $H_{||}$ and formation of a sharp flux front, delaying the entry of new vortices across $H_{||}$. We associated the novel observed flux patterns, similar to those reported earlier in [3], with the layered structure of YBCO, forcing the motion of the incoming pancake vortices along the Josephson-like, in-plane flux lines, and with the cutting processes of the in-plane and new entering vortices.. The simulations of the crossing process in [2] revealed time variations of the vortex shape and allowed us to conclude that defects can increase the flux crossing barrier due to the pinning of strongly bent segments of intersecting vortices, and hence enhance currents along the crossing flux fronts.

In principle, the anisotropic dynamics of different flux components in thin plates of any type II superconductor (both isotropic and anisotropic, homogeneous and layered), defined by the thin plate geometry, was predicted by Brandt [4], where he considered effects of the Meissner currents induced by the crossing external fields on the changing shape of vortices and showed that various flux diffusivities occur along different in-plane directions depending on the plate shape and the field orientation. Later, [5] he discussed possible physical reasons for the anisotropic normal flux motion in thin superconducting plates magnetized with an in-plane field. One mechanism of the anisotropic vortex dynamics is based on circulating Meissner currents , J_M, induced by the normal magnetic field $H_\perp$. In a long rectangular plate with in-plane vortices generated by the longitidinal magnetic field $H_{||}$, the Meissner current due to $H_\perp$ is perpendicular to the $H_{||}$ vortices at the short ends of the plate. The resulting Lorentz force bends the tails of the in-plane vortices towards $H_\perp$. In contrast, along the long edges of the plate, J_M is parallel to the $H_{||}$ vortices keeping them intact. Consequently, the vortex bending mode propagates from the short ends along $H_{||}$ towards the middle of the plate. Another mechanism is the crossing-reconnection of the perpendicular to the plane and in-plane vortices, which can delay the entry of $B_\perp$ near the longitudinal edges. Both mechanisms result in much faster entry of the normal vortices along $H_{||}$ than across it. In the above picture, the normal flux entry along $H_{||}$ should start with asymmetric bending of vortices with respect to the plate plane. In our previous experiments, we observed the anisotropic but symmetric entry of $B_\perp$ in a YBCO crystal magnetized with $H_{||}$ and explained the symmetry accounting for the layered structure of the sample, where mobile pancake vortices carry the normal flux along Josephson-like longitudinal flux lines [2].

In this work we study the entry of $B_\perp$ in isotropic superconducting Nb films magnetized by a relatively large in-plane field at temperatures of the slow uniform vortex dynamics ($T>T_C/2$) and at lower temperatures ($<T_C/2$), when the normal flux motion is dominated by thermo-magnetic avalanches (TMA). The magneto-optical images reveal essentially anisotropic normal flux dynamics in a 200 nm thick Nb film. We observe advanced <<faster or accelerated>> uniform vortex motion along $H_{||}$ at $T>T_C/2$ and preferential thermo-magnetic jumps perpendicular to $H_{||}$ at $T<T_C/2$. In contrast, we find virtually no anisotropy in a 100 nm thick Nb film. The pronounced dissimilar vortex dynamics can be associated with the presence and absence of in-plane vortices in the 200nm and 100nm film, respectively, and with the different tilting behavior of vortices in these two films induced by the perpendicular field. The vortex crossing-reconnection processes in the thicker film, responsible for retarding normal flux propagation across $H_{||}$, and the isotropic pinning of tilted vortices in the thinner film, can explain the difference in the observed flux patterns. Our study shows that vortex crossing effects can introduce *qualitative* changes in the flux dynamics, which can be used to tailor vortex dynamics in superconducting films.

Experiment

In this work we used magneto-optic imaging technique based on garnet indicator films [6] to visualize the normal-to-surface flux penetration in Nb films in the presence of an additional magnetic field parallel to the field plane. Two Nb films of different thickness, 100 nm and 200 nm, were deposited on oxidized silicon substrates using high-vacuum DC magnetron sputtering. The square shaped samples with T_c=8.7K (2x2mm, 100 nm film) and

T_c=9K (2.5x2.5mm, 200 nm film) displayed sharp superconducting transitions ($\Delta T \sim 0.1K$) obtained by magnetization measurements in a small, ~5 Oe, perpendicular field. The magneto-optic imaging experiment was carried out in an optical closed-cycle cryostat (Montana instruments). The film was overlayed with a garnet indicator film allowing real time observation of the normal flux distribution under a polarized light microscope. The samples were cooled below T_C in a field of $H_{||}$ = 965 Oe, oriented along any chosen direction in the film plane, and a perpendicular field $H_\perp$ was slowly ramped up in the presence of the parallel field $H_{||}$. Images of the normal (out-of-plane) flux patterns, $B_\perp$, over the sample area were recorded with a field-cooled 16 bit CCD camera. The strict alignment of $H_{||}$ in the film plane was determined by the total disappearance of the magneto-optical $B_\perp$ signal at T>T_C. Below, we present illustrations of the normal flux evolution at temperatures ranging from 3.5 to 8K, in the 200 nm thick Nb film. highlighting the anisotropic vortex patterns anisotropic with respect to $H_{||}$. At the end of the next section, we will show the isotropic $B_\perp$ patterns observed in the presence of the same $H_{||}$ field for the 100 nm thick Nb film.

Normal flux patterns in the presence of the in-plane field

(a) T>T_C/2. Smooth flux entry (200 nm Nb film).

To distinguish the effect of the in-plane field $H_{||}$ on the entry of $B_\perp$ we will first discuss the normal flux patterns in the absence of $H_{||}$ shown in Fig.1 for the 200nm thick Nb film. Qualitatively, at T≥T_c/2 the entry of the perpendicular field $B_\perp$ into the film follows a classic scenario. First, an applied normal magnetic field (bright contrast) concentrates at the perimeter of the film due to the induced Meissner currents . With increasing $H_\perp$ the normal flux smoothly penetrates the film in the shape of $B_\perp$ lobes extending from the edges towards the center of the square (Fig.1a-b). Such penetrating normal flux structures are typical for thin superconducting films and reflect the fractal dynamics of vortices moving through a network of defects [7-8]. The vortex lobes can be associated with "magnetic flux jets" initiating at defects and protruding in the vortex propagation direction at distances much larger than the defect size due to the strongly nonlinear superconducting current flow [9]. The overlapping vortex lobes form a characteristic pillow-shaped pattern with arched $B_\perp$ flux fronts defined by the shape of the sample (Fig.1a-b). With increasing $H_\perp$, the penetrating $B_\perp$ fronts merge and form an envelope pattern, representing the total critical state (Fig.1c) where the flux has penetrated the entire sample. It has minimum $B_\perp$ (dark contrast) along the diagonals of the square where the critical currents flowing along the sample edges sharply turn and yield the strongest screening of the applied field. Perfect alignment of the maximum screening lines along the square diagonal confirms that the sample is homogeneous and isotropic in the film plane. When $H_\perp$ is decreased, the direction of the screening currents reverse and the envelope pattern inverts showing the maximum trapped flux (bright contrast) along the square diagonals (Fig.1d).

The application of $H_\perp$ to a Nb-film cooled in an in-plane field of $H_{||}$=0965 Oe, shows generally similar behavior to the case of $H_{||}$=0. However, $H_{||}$ results in a noticeable anisotropy of the normal flux dynamics with faster propagation of $B_\perp$ along the in-plane field direction. Figs.2a-b show $B_\perp$ patterns when $H_{||}$ is oriented along one of the square sides. Here, the

penetrating normal flux lobes are longer along $H_{||}$ and shorter in the perpendicular direction. In the total critical state (Fig.2c), achieved at $H_\perp$ =220 Oe, the maximum screening lines do not follow the square diagonals as shown in Fig. 1c, but instead, form a stretched envelope pattern, corresponding to increased critical currents along $H_{||}$. Reducing $H_\perp$ to zero inverts the trapped flux pattern keeping the same stretched envelope shape (Fig.2d). Similar pictures but rotated by $\pi/2$ are observed when the in-plane field is rotated by $\pi/2$, indicating that flux pinning is uniform in this film.

Estimates of the ratio of the critical currents along and across $H_{||}$ from the envelope patterns in Fig.2c-d yield $J_c^{||}/ J_c^\perp$ =1.4 . Interestingly, this ratio remains the same from T=5K to 8.3K. At lower temperatures the flux patterns are strongly distorted by TMA as discussed below, and the current ratio cannot be quantified.

When the in-plane field is oriented along one of the square diagonals, in the increasing $H_\perp$ we still observe the extension of the normal vortex lobes towards $H_{||}$ caused by the preferential motion of vortices in that direction (Fig.3a-b). There is some finite angle difference between the flux lobe direction and $H_{||}$ because critical currents flowing along the sample edges deflect the vortex trajectories toward the sample center. In the total critical state, both penetrating and trapped flux patterns (Fig.3c-d) show maximum screening lines along the square diagonals, similar to $H_{||}$ = 0 case. Obviously, in the case of diagonally applied $H_{||}$, we have the same density of currents flowing along the sample perimeter in spite of different angles between the extending vortex lobes and crossing diagonals. As a result, the currents lines make sharp turns at the square diagonals. Similar behavior is observed when $H_{||}$ is applied along another square diagonal direction.

(b) $T \leq T_C/2$. Thermo-magnetic avalanches (200 nm Nb film).

Below ~Tc/2, in contrast to the smooth flux entry, we observe jump-wise intermittent appearance of dendritic vortex patterns (Fig.4a) associated with the emergence of thermo-magnetic instabilities [10-12]. The thermo-magnetic avalanches (TMA) are triggered by the fast motion of vortices which has broken free of a strong pinning barrier (in this case, the edge barrier), causing large dissipation of energy and local heating along their path. The local heating enhances the mobility and boosts the speed of the successive vortices, ultimately resulting in the dramatic flux jumps. The overheated channels of the vortex jumps, where temperatures can rise above T_C , disrupt the laminar current flow and form Lichtenberg patterns similar to those observed in electric breakdown discharge [13]. The branching depends on the cooling conditions, geometry, and the defect structure of the sample. Fractal-like patterns are typical for thin films [14-17], although fingering was observed also in bulk superconducting disks [18]. For $H_{||}$ = 0, new flux branching patterns intermittently jump from all the edges towards the middle of the sample with increasing $H_\perp$ until the entire square is covered with an intricate, but on average, symmetric network of enhanced $B_\perp$ lines (Fig.4a-c). At larger $H_\perp$ fields, the lines smooth out, resulting in the usual critical state envelope pattern (not shown) similar to that in Fig.1c. With subsequent decrease of $H_\perp$ from a maximum value of 662 Oe, negative normal flux dendrites jump from the edges, forming a complex network of negative $B_\perp$ branches (fig.4d).

Based on the enhanced mobility of vortices along the in-plane field $H_{||}$ for $T>T_c/2$ discussed earlier, one would expect the preferential extension of the dendritic flux patterns along $H_{||}$. In contrast, we found that the advanced growth of the dendrite branches occurs perpendicular to the $H_{||}$ direction. At the initial stage of magnetization, the dendrites appear preferentially on sides of the sample that are parallel to $H_{||}$ and expand in the direction perpendicular to $H_{||}$ (Fig.5a). Interestingly, the tendency for the advanced dendrite growth perpendicular to $H_{||}$ becomes stronger with increasing temperature from 3.2 to 5K (see below the discussion of the 5K flux patterns). This trend extends to larger $H_{\perp}$ where the dendrite branches occupy most of the sample area (Fig.5b-c). Similar anisotropy is observed in negative $B_{\perp}$ dendrite patterns formed when decreasing $H_{\perp}$ to 0 (Fig.5d).

When $H_{||}$ is applied along a diagonal of the square, with increasing $H_{\perp}$ flux dendrites emerge with the same probability at all sample sides (Fig.6a-b). However, their branches are not extended towards the center of the sample but turn noticeably across $H_{||}$. The same tendency is observed at larger $H_{\perp}$ (Fig.6c) and in the subsequent pattern formed after reducing $H_{\perp}$ from a maximum value to 0 (Fig.6 d).

Fig.7 summarizes the experimental results delineating the effect of an in-plane field on the penetration of normal vortices for the 200nm thick Nb film in both the regime of TMA and at smooth normal flux entry as observed at an intermediate temperature of 5K. At this temperature, the flux dendrites emerge at small values of $H_{\perp}$ (see the top two rows in Fig.7 showing results for $H_{||}=0$ and $H_{||}=965$ Oe for 0, $\pi/2$, and $3/4\pi$) and the uniform critical state forms at larger normal fields (third row in Fig.7). Similar to patterns observed at T<5K, the dendrites preferentially emerge from the edges of the film that are parallel to the in-plane field and their branches tend to grow across $H_{||}$. At the same time, similar to the behavior at larger T, the smooth entry of the normal flux is advanced along the in-plane field direction and results in the appropriate critical state envelope structures.

(c) *Flux patterns in the 100 nm Nb film*.

In the 100 nm thick Nb film, we do not see any noticeable anisotropy due to $H_{||}$ in the flux dynamics at any temperature as illustrated in Fig.8. Unlike in the 200 nm film, neither the flux lobes of $B_{\perp}$ extending perpendicular from the edges at smaller $H_{\perp}$ (Fig.8 left column), nor the diagonal patterns of the total critical state for increasing (Fig.8 middle column) and decreasing field (Fig.8 right column) show any deformation from the symmetry defined by the square geometry. Also, we do not see any anisotropy in the TMA patterns (not shown). Here, the TMA develops at slightly lower temperatures and flux jumps are less frequent than in the thicker film, which may be associated with the more efficient heat transfer to the substrate in the 100 nm film.

Discussion

(a) In-plane vortices

Here we consider possible reasons for the effect of the in-plane field on the normal flux dynamics in 200 nm Nb film and discuss causes for the different behavior observed in the 100

nm film.

Based on the measured resistivity ρ(9.5K) and relationship ρl =3.72×10^{-6} $\mu\Omega$ cm^2 for Nb [19] our films have mean free path l =9nm; then $\lambda(0)=\lambda_0(\xi_0/l)^{1/2}$ =84nm and $\xi(0)= (\xi_0 l)^{1/2}$ = 19nm with ξ_0=39nm and λ_0=39nm for bulk Nb (see e.g. [20]). These are typical values for magnetron sputtered Nb films of similar thickness: $\lambda(0)\sim$50-90nm and the coherence length $\xi(0)\sim$10-20nm. So both films are thicker than the penetration depth λ . However, the first critical field for the appearance of longitudinal vortices in these films, which is strongly dependent on the film thickness d, could be quite different. Estimates of $H_{c1\parallel}$ using above values of λ and ξ (λ=84nm and ξ=19nm) and exact Abrikosov's formula for films in parallel fields [21]:

$$H_{c1}=(\Phi_0/4\pi\lambda^2)[K_0(\lambda/\xi)- 2\Sigma_{n=1}^{\infty} (-1)^n K_0(n\lambda/d)][\cosh (d/2\lambda)/(\cosh (d/2\lambda)-1)] \qquad (1)$$

yield $H_{c1}\sim$1200 Oe for the d=100nm thick film and $H_{c1}\sim$600 Oe for the d=200nm film . To confirm that in-plane vortices can be formed only in the thicker film, we calculated numerically the in-plane vortex Gibbs potential, G, as a function of the vortex period a, for the 100nm and 200nm films at $H_\parallel$ =1 kOe using the results of [22]:

$$G(a) = \frac{1}{a}\left(\frac{H_V(0)\Phi_0}{8\pi} - \frac{H_\parallel\Phi_0}{4\pi}\left[1 - \frac{\cosh (u/\lambda)}{\cosh (d/2\lambda)}\right]\right) \qquad (2)$$

where

$$H_V(0) = \frac{\Phi_0}{2d\lambda}\sum_{n=1}^{\infty} \frac{\left(1-(-1)^n \cos\frac{2\pi nu}{d}\right)\cosh\left(v_n\frac{a-\xi}{\lambda}\right)+\left(\cos\frac{2\pi nu}{d}-(-1)^n\right)\cosh\left(v_n\frac{\xi}{\lambda}\right)}{v_n \sinh\left(v_n\frac{a}{\lambda}\right)} \qquad (3)$$

$v_n = \sqrt{1 + (n\pi\lambda/d)^2}$ and u=0 for the one row in-plane vortex array.

 The resulting plots of G(a) for λ=84nm and ξ=19nm are presented in Fig.9 , which shows that the minimum in G(a) corresponding to a$\sim$2λ appears only in the 200nm thick film. G(a) for the 100nm thick film changes monotonously and is positive throughout. With increasing temperature from 4 to 8K the penetration depth should increase by a factor of 1.6 in accordance with the two-liquid model. At this larger λ (and ξ(8K)$\sim$1.6ξ(4K)) the curves for G(a) shift slightly down, but the minimum of the Gibbs potential remains only in the thicker film (see Supplementary Material). Consequently, in the 100nm film, our field of $H_\parallel$=965 Oe can be insufficient for nucleation of vortices while in-plane vortices can form in the 200nm film. Thus, in our experiment, the normal vortices generated by $H_\perp$ should encounter in-plane vortices only in the 200nm film. In the 100nm film there will be spatially homogeneous in-plane fields smoothly decaying from both film surfaces along the normal axis z and slightly screened compared to the external $H_\parallel$ as (see e.g. [23-24]):

$$B_\parallel = H_\parallel \cosh(z/\lambda)/\cosh(d/2\lambda) \qquad (4)$$

(b) Vortex cutting in crossing fields

The presence of in-plane vortices in the 200nm thick film and their absence in the 100nm thick film can explain the observed differences in the $B_\perp$ flux dynamics. According to our earlier observations in YBCO crystals [2] and simulations using Ginzburg-Landau formalism [25-26], the vortex crossing in the presence of pinning can effectively delay the vortex motion. Therefore, the crossing-reconnection effects, which in this case occur in the thicker film, should delay the motion of normal $B_\perp$ vortices moving *across* the $H_{||}$ direction, while their motion *along* $H_{||}$ should not be impeded by the vortex crossing. In the thinner film, the motion of the $B_\perp$ vortices in both directions is hindered only by pinning and should be isotropic.

The crossing-reconnection of the in-plane and tilted vortices and the enhanced pinning of vortices with increased tilt angle, both boosting the critical currents along $H_{||}$ and thus the gradient of $B_\perp$ across $H_{||}$, can also explain the directionality of the dendritic TMA patterns at $T<T_c/2$. Similar to granular avalanches, vortex avalanches follow the steepest slopes of the potential relief, formed in the latter case by pinning. Enhanced pinning is a natural requirement for the appearance of vortex avalanches. In a sample with weak pinning and thus acting on vortices small critical currents, the shallow flux gradients can smoothly relax through the thermal creep. Similarly, large critical currents resulting from strong pinning can provide fast acceleration of vortices to nucleate TMAs. Therefore, stronger pinning for the vortex motion across $H_{||}$ can define the preferential appearance of dendrites on the sides parallel to $H_{||}$ and the directional growth of their branches across $H_{||}$.

(c) Vortex angle in tilted fields

Another possible explanation of the difference in the normal flux behavior in our films can be the strong change in the tilt angle of vortices entering with increasing $H_\perp$. To estimate the tilt of entering vortices in the 100nm film, we used formular for the vortex shape X(z) from [23], which gives correct vortex description for films with $d \geq \lambda$:

$$X(z) = tz - tl\frac{sinh(\frac{z}{l})}{\cosh(\frac{d}{2l})} \qquad\qquad (5)$$

Here $l \approx \lambda$, t =$(H_{||}/H_\perp)(\pi\lambda/a)^2/[\ln\kappa +1/2]$, $\kappa=\lambda/\xi$, *a* is the distance between vortices, and we accepted the anisotropy factor $\Gamma=1$.

Fig.10 shows the shape of vortex lines in the films of thickness $d=\lambda$ and $d=2\lambda$ and reveals a considerable change in the vortex tilt angle as the film thickness increases. In the calculations, we assumed the distance between vortices $a\sim\lambda$ and the anisotropy coefficient $\Gamma=1$. Note, that the X-coordinate in Fig.10 is shown for $H_{||}/H_\perp =1$, and it should be multiplied by the experimental ratio of the in-plane and normal fields ($H_{||}/H_\perp \sim 10$ in our case). But even with this factor, the vortex tilt angle still remains $< 40^0$ from the normal for the 100 nm thick film and is ~twice larger for the 200 nm thick film. Basically, the same description of the individual vortex shape in the films is obtained using eq.7 of [27]. In the limit of small $d<<\lambda$

the vortex shape depends only on d, i.e. it is independent of λ and thus on temperature. A weak dependence on λ and thus on T remains for d ~λ. The penetration depth will increase by a factor of 1.6 with increasing temperature from 4 to 8K. In a film of a given thickness the average tilt will moderately decrease. However, there will be still a large difference in the vortex tilt between the films of the thickness d and 2d (see Supplementary Material). Such weak temperature dependence is in accordance with our observations of the unchanged anisotropy of the normal flux dynamics from 5 to 8K, if this anisotropy is defined by the mutual angle of the tilted and in-plane vortices.

(d) Geometrical factor for pinning of tilted fields

If we account for the tilt angle of the entering $B_\perp$ vortices, the anisotropy in their motion across and along the tilt plane can be expected due to the effect of pinning from the different areas swept by vortices moving along and across $H_{||}$ (see scheme in Fig.11). If a vortex tilted by angle θ from the film normal moves by a distance *b* in the tilt plane, it traverses an area s1~*b*d. However, when it moves by the same distance perpendicular to the tilt plane, the swept area is s2~bd/cosθ > s1 and thus the vortex interacts with a larger number of pinning centers, admitting a homogenous pinning landscape. Then the vortex motion across $H_{||}$ should be slower than along $H_{||}$ and the anisotropy will increase as 1/cosθ. If we assume that in the 100nm thick film, the tilt angle of entering $B_\perp$ vortices is actually smaller than discussed above, and they remain nearly perpendicular to the film surface, then the anisotropy of the normal field penetration should be very small and it should be noticeably larger for the 200nm film. However, the fact that the anisotropy observed in the 200nm film does not change with temperature, indicates that the effect of pinning (supposed to decrease with T) is probably not the dominant factor in the vortex motion anisotropy.

(e) Tilted mode propagation

An interesting scenario explaining the difference in the normal flux propagation in a superconducting strip magnetized by an in-plane field was suggested by Brandt [4, 5]. Application of a normal field to a strip containing longitudinal in-plane vortices should tilt the vortex tails near the strip edges perpendicular to $H_{||}$, where the screening currents induced by $H_\perp$ are perpendicular to vortices. This vortex tilt will preferentially propagate along $H_{||}$ towards the sample center upon increasing $H_\perp$. At the same time, the screening currents near the edges parallel to $H_{||}$ flow along the in-plane vortices (force-free configuration) leaving them undisturbed. This should result in a noticeable normal flux entry anisotropy from different edges of the strip. In our case, the above scenario is probably not relevant because the anisotropy observed in the 200 nm film is only 1.4 and in Brandt's picture it is expected that the tilt mode propagation should be temperature dependent.

We believe that the presence of the in-plane vortices and their inevitable cutting and reconnection with the tilted vortices induced by the perpendicular field is the major reason of the observed anisotropy of the normal flux penetration in the 200nm film. In turn, the isotropy of the normal vortex motion in the 100nm film is associated with the absence of in-plane vortices for finite $H_{||}$. In principle, the structure of the tilted vortices in thin films

changes across the film thickness, and their description as flexible lines is approximate. Also, the crossing-reconnection process is not well understood even for vortices in bulk superconductors [1]. Albeit, our recent simulations show [25, 26] that the vortex cutting can effectively delay the penetration of crossing vortices into the sample. Previous reports of crossing-fields in thin YBCO plates [2, 3], and the anisotropy of the vortex dynamics in the thicker Nb film can be an experimental confirmation of this conjecture.

Conclusions

Observations of the normal-to-plane flux propagation in superconducting films with in-plane magnetization reveal a considerable anisotropy of the normal vortex dynamics in the thicker film and isotropic normal vortex motion in the thinner film. At temperatures $T>T_c/2$, the smooth normal vortex entry into the thicker film is preferential along the in-plane field $H_{||}$. At $T<T_c/2$ the normal flux entry is dominated by dendritic patterns of the thermomagnetic jumps, which in the thicker film stretch preferentially across the $H_{||}$ direction, whereas they are independent of $H_{||}$ in the thinner film.

The observed anisotropy of the normal flux dynamics at $T>T_c/2$ in the thicker film is a result of vortex crossing-reconnection, which can delay the motion of the tilted vortices generated by $H_\perp$ across the in-plane vortices induced by $H_{||}$. In contrast, the in-plane vortices are absent in the thinner film at finite values of $H_{||}$ and tilted vortices are aligned close to the film normal, which results in isotropic normal flux dynamics. Here, one may expect that with increasing in-plane field above H_{c1} to nucleate longitudinal vortices in the thinner film, it may be possible to also induce anisotropy in the normal flux dynamics.

The same mechanism explains the tendency of the TMAs to branch across the $H_{||}$ direction at $T<T_c/2$ in the thicker film. For the TMA, the preferential direction of the dendrite growth is across the in-plane vortices, which form an obstacle for the motion of normal flux across them due to flux cutting and reconnection and thus increase the critical current parallel to the $H_{||}$ direction. The enhanced currents form a steeper potential relief for vortex motion across this direction as compared to the other, hence defining the preferential direction of the vortex jumps perpendicular to $H_{||}$.

We believe our results shed new light on the vortex cutting phenomenon, which is poorly understood in bulk and basically unexplored in thin film superconductors, and still awaits thorough experimental and theoretical research.

Acknowledgements

References
[1] A. M. Campbell, SUST **24**, 091001 (2011). Flux cutting in superconductors.

[2] V. Vlasko-Vlasov, A. Koshelev, A. Glatz, C. Phillips, U. Welp, and W. Kwok, Phys. Rev. B **91**, 014516 (2015). Flux cutting in high-Tc superconductors.

[3] M. V. Indenbom, A. Forkl, B. Ludescher, H. Kronmuller, H.-U. Habermeier, B. Leibold, G. D'Anna, T. W. Li, P. H. Kes, and A. A. Menovsky, Physica C **226**, 325 (1994). Anisotropy of perpendicular field penetration into high-Tc superconductors induced by strong longitudinal field.

[4] E. H. Brandt, Phys. Rev. Lett. **68**, 3769 (1992). Double Peaks in the Dissipation of Vibrating Superconductors,

[5] E. H. Brandt, Rep. Progr. Phys. **58**, 1465 (1995). The flux-line lattice in superconductors. §7.3.

[6] V. K. Vlasko-Vlasov, G. W. Crabtree, U. Welp, and V. I. Nikitenko, NATO Advanced Science Institutes Series, Series E, Applied Sciences **356**, 205 (1999). Magneto-Optical Studies of Magnetization Processes in High-Tc Superconductors.

[7] R. Surdeanu, R. J. Wijngaarden, E. Visser, J. M. Huijbregste, J. H. Rector, B. Dam, and R. Griessen, Phys. Rev. Lett. **83**, 2054 (1999). Kinetic Roughening of Penetrating Flux Fronts in High-Tc Thin Film Superconductors.

[8] V. K. Vlasko-Vlasov, U. Welp, V. Metlushko, and G. W. Crabtree, Phys. Rev. B **69**, 140504R (2004). Experimental test of the self-organized criticality of vortices in superconductors.

[9] M. Friesen, A. Gurevich, Phys. Rev. B **63**, 064521 (2001). Nonlinear current flow in superconductors with restricted geometries.

[10] R. G. Mints, A. L. Rakhmanov, Rev. Mod. Phys. **53**, 551 (1981). Critical state stability in type-II superconductors and superconducting-normal-metal composites.

[11] S. L. Wipf, Cryogenics **31**, 936 (1991). Review of stability in high temperature superconductors with emphasis on flux jumping,

[12] E. Altshuler, T. H. Johansen, Rev. Mod. Phys. **76**, 471 (2004). Colloquium: Experiments in vortex avalanches.

[13] N. Femia, L. Niemeyer, V. Tucci, J. Phys. D **26**, 619 (1993). Fractal characteristics of electrical discharges: experiments and simulation.

[14] P. Leiderer, J. Boneberg, P. Brull, V. Bujok, S. Herminghaus, Phys. Rev. Lett. **71**, 2646 (1993). Nucleation and growth of flux instability in superconducting YBa2Cu3O7-x films.

[15] T. H. Johansen, M. Baziljevich, D. V. Shantsev, P. E. Goa, Y. M. Galperin, W. N. Kang, H. J. Kim, E. M. Choi, M. S. Kim, S. I. Lee, SUST **14**, 726 (2001). Dendritic flux patterns in MgB2 films.

[16] F. Colauto, E. J. Patino, M. G. Blamire, and W. A. Ortiz, SUST **21**, 045018 (2008). Boundaries of the instability region on the HT diagram of Nb thin films.

[17] F. Colauto, M. Motta, A. Palau, M. G. Blamire, T. H. Johansen, and W. A. Ortiz, IEEE Trans. .Appl. Supercond. **25**, 7500704 (2015). First Observation of Flux Avalanches in a-MoSi Superconducting Thin Films.

[18] M. R. Wertheimer, J. le G. Gilchrist, J. Phys. Chem. Sol. **28**, 2509 (1967). Flux jumps in type II superconductors.

[19] A. F. Mayadas, R. B. Laibowitz, J. J. Cuomo, J. Appl. Phys. **43**, 1287 (1972). Electrical Characteristics of rf-Sputtered Single-Crystal Niobium Films.

[20] G. Carapella, P. Sabatino, G. Costabile, J. Appl. Phys. **111**, 053912 (2012). Considerable asymmetry of the critical current in a niobium thin strip of plano-convex section.

[21] A. A. Abrikosov, Fundamentals of the Theory of Metals (Elsevier Science Publisher, Amsterdam, 1988 .

[22] D. A. Luzhbin, Phys. Sol. State **43**, 1823 (2001). Structure of the Abrikosov Vortex Lattice in a Thin Superconducting Film in a Parallel Magnetic Field.

[23] E. H. Brandt, Phys. Rev. B **48**, 6699 (1993). Tilted and curved vortices in anisotropic superconducting films.

[24] Yu. A. Martynovich, JETP **78**, 489 (1994). Magnetic vortices in layered superconducting slabs.

[25] V. K. Vlasko-Vlasov, A. Glatz, A. E. Koshelev, U. Welp, and W. K. Kwok, Phys. Rev. B **91**, 224505 (2015). Anisotropic superconductors in tilted magnetic fields.

[26] A. Glatz, V. K. Vlasko-Vlasov, W. K. Kwok, G. W. Crabtree, Phys. Rev. B **94**, 064505 (2016). Vortex cutting in superconductors.

[27] D. A. Savinov, SUST **25**, 015003 (2012). Magnetic field imaging of curved vortex lines in thin films of anisotropic superconductors.
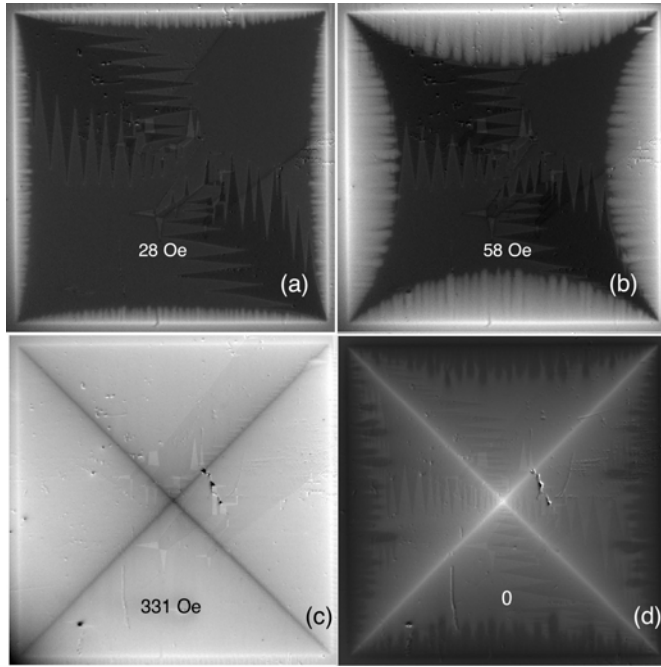
Figures and captions

Fig.1 Normal flux patterns in 2.5x2.5mm square sample of 200 nm thick Nb film at 6K in the absence of the in-plane field. (a-c) magneto-optic images in the increasing normal field $H_\perp$, (d) trapped flux pattern after reducing field to zero from maximum of 662 Oe. Values of $H_\perp$ are shown on the pictures. The brightness of the magneto-optic contrast corresponds to the normal flux density. Zigzag structures across the image in (d) correspond to the in-plane domain walls in the garnet indicator film.
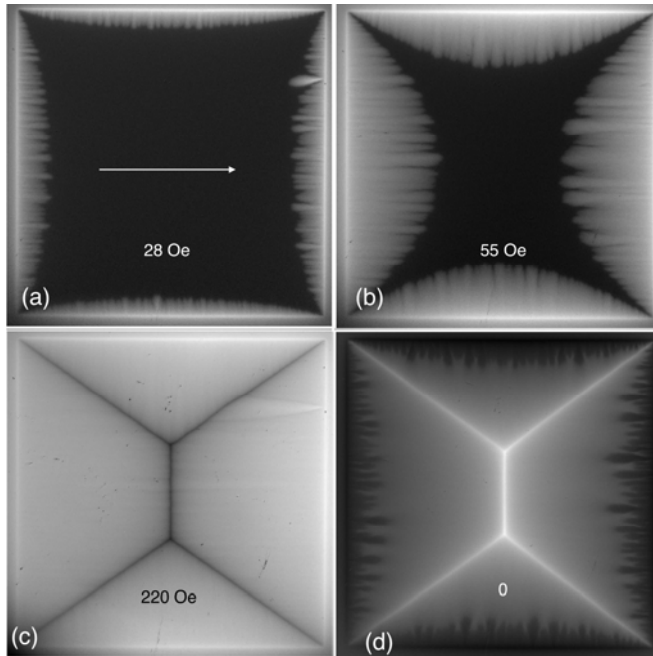
Fig.2 Same as Fig.1 in the presence of the in-plane field $H_{||}$=965 Oe along the horizontal side of the square. T=6K. Values of $H_\perp$ are shown on the pictures. Arrow shows the direction of $H_{||}$.
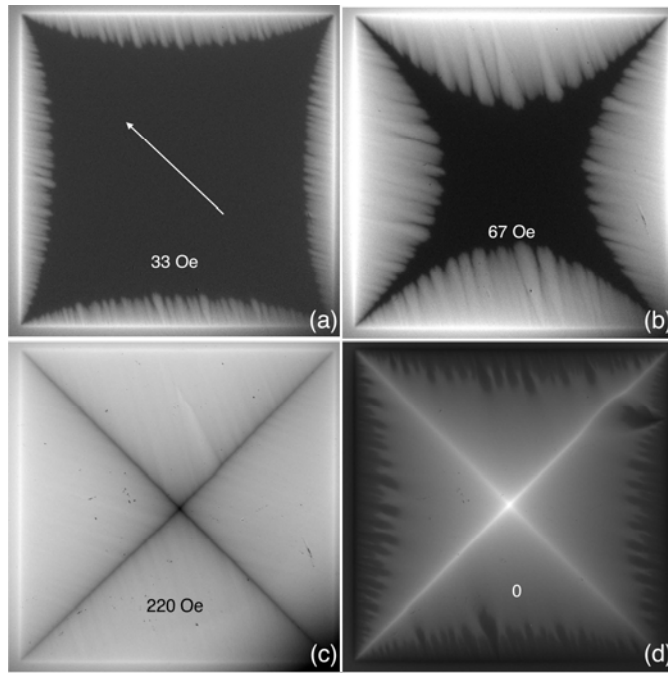
Fig.3 Same as Fig.1 in the presence of the in-plane field $H_{||}$=965 Oe along one of diagonals of the square. T=6K. Values of $H_\perp$ are shown on the pictures. Arrow shows the direction of $H_{||}$.
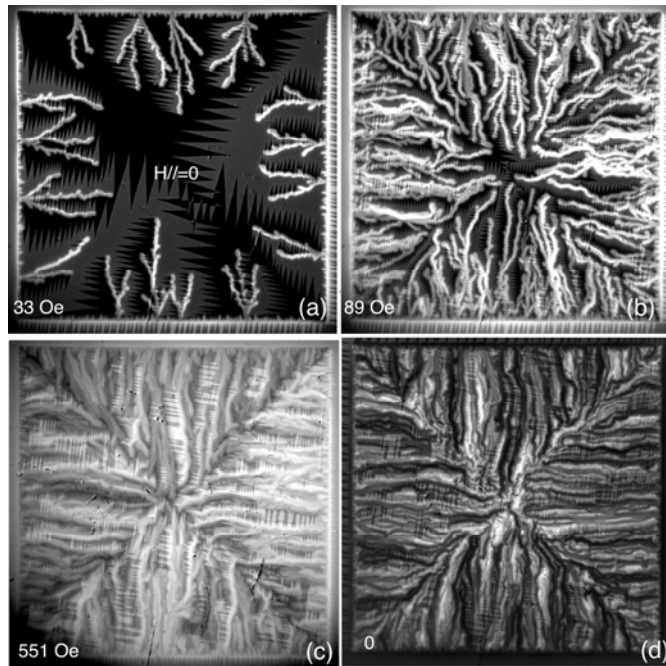
Fig.4 Dendritic patterns due to the thermo-magnetic avalanches (TMA) in the absence of the in-plane field at T=3.2K. New branching dendrites with increased $B_\perp$ (bright) jump intermittently but symmetrically from all sides of the square with increasing $H_\perp$. (a-c) increasing $H_\perp$ and (d) trapped flux pattern with negative $B_\perp$ (dark) dendrites formed at decreasing $H_\perp$ from maximum of 662 Oe. Values of $H_\perp$ are shown on the pictures.
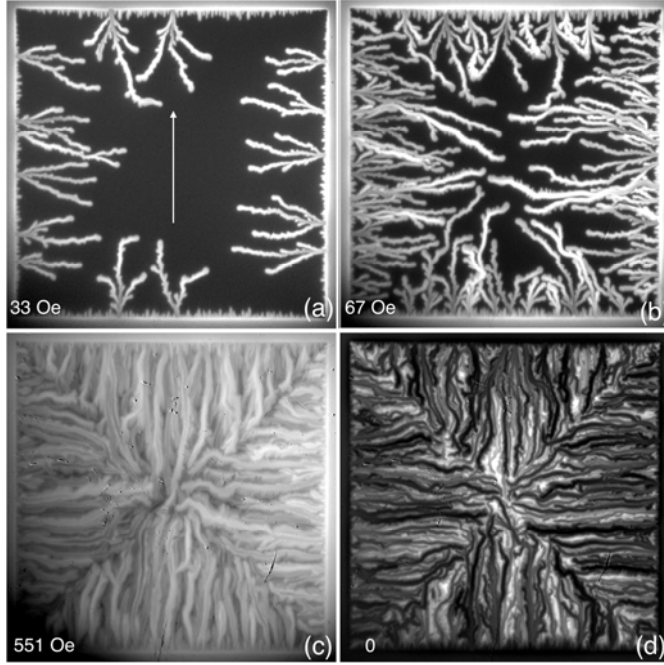
Fig.5 TMA patterns at T=3.2K in the presence of $H_{||}$=965 Oe along the vertical side of the square. (a-c) increasing $H_\perp$ and (d) trapped flux pattern showing negative dendrites formed at decreasing $H_\perp$. Values of $H_\perp$ are shown on the pictures. Arrow shows the direction of $H_{||}$. Dendrites are preferentially generated on the square sides parallel to $H_{||}$ and have longer branches across $H_{||}$.
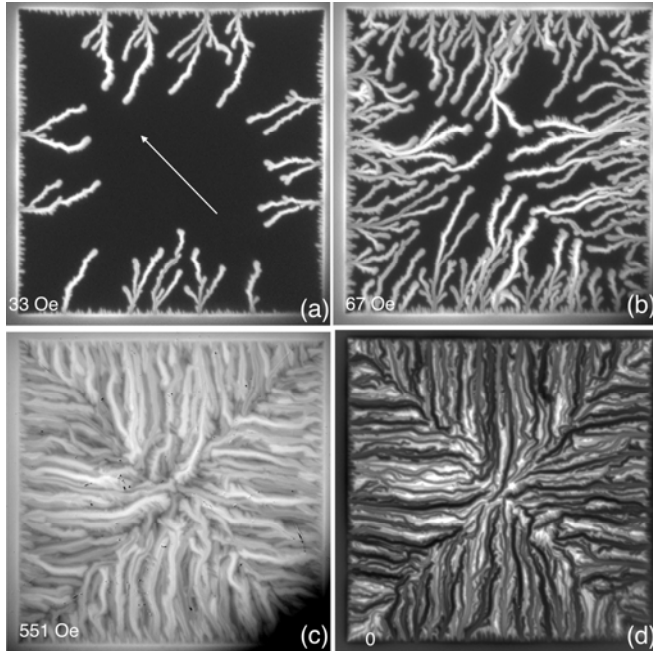

Fig.6 TMA patterns at T=3.2K in the presence of $H_{||}$=965 Oe along one of diagonals of the square. (a-c) increasing $H_\perp$ and (d) trapped flux pattern with negative dendrites. Values of $H_\perp$ are shown on the pictures. Arrow shows the direction of $H_{||}$. Dendrites are generated symmetrically on all square sides but their branches tend to turn across $H_{||}$.
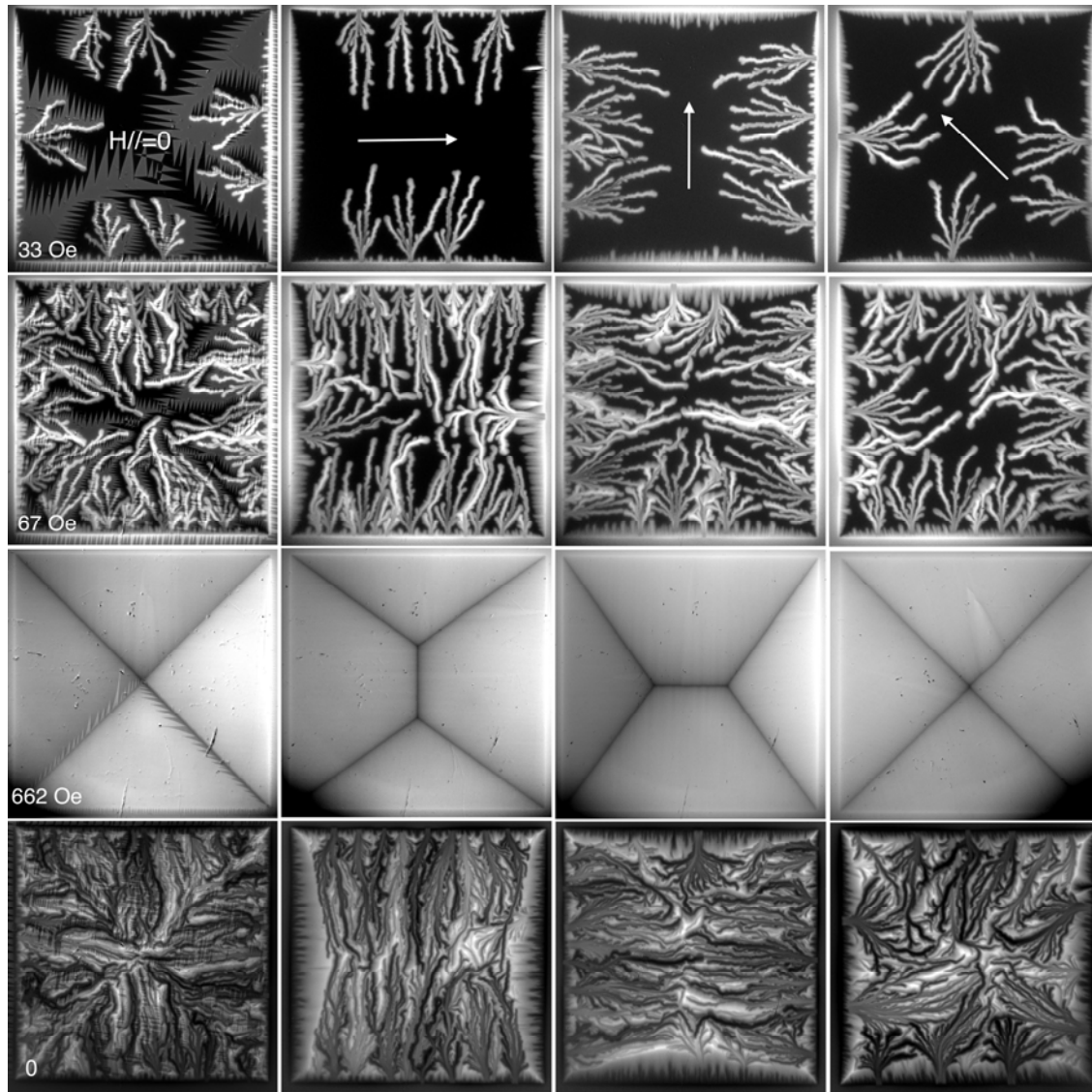
Fig.7 Dendritic and smooth flux patterns observed in 200nm Nb film at T=5K in the presence of in-plane field $H_{||}$ applied along different directions. First column of pictures presents data for $H_{||}=0$. Next three columns show patterns for orientations of $H_{||}$ indicated by arrows in the top picture of each column. Values of $H_\perp$, the same for each row, are shown near the first column. At 5K TMA jumps occur at lower $H_\perp$ followed by the smooth normal flux entry at larger $H_\perp$. The smooth $B_\perp$ penetration wipes out the dendritic structures and results in a regular critical state pattern shown in the third from top row. The bottom row presents trap flux patterns with negative $B_\perp$ dendrites generated at decreasing $H_\perp$ from maximum of 662 Oe.
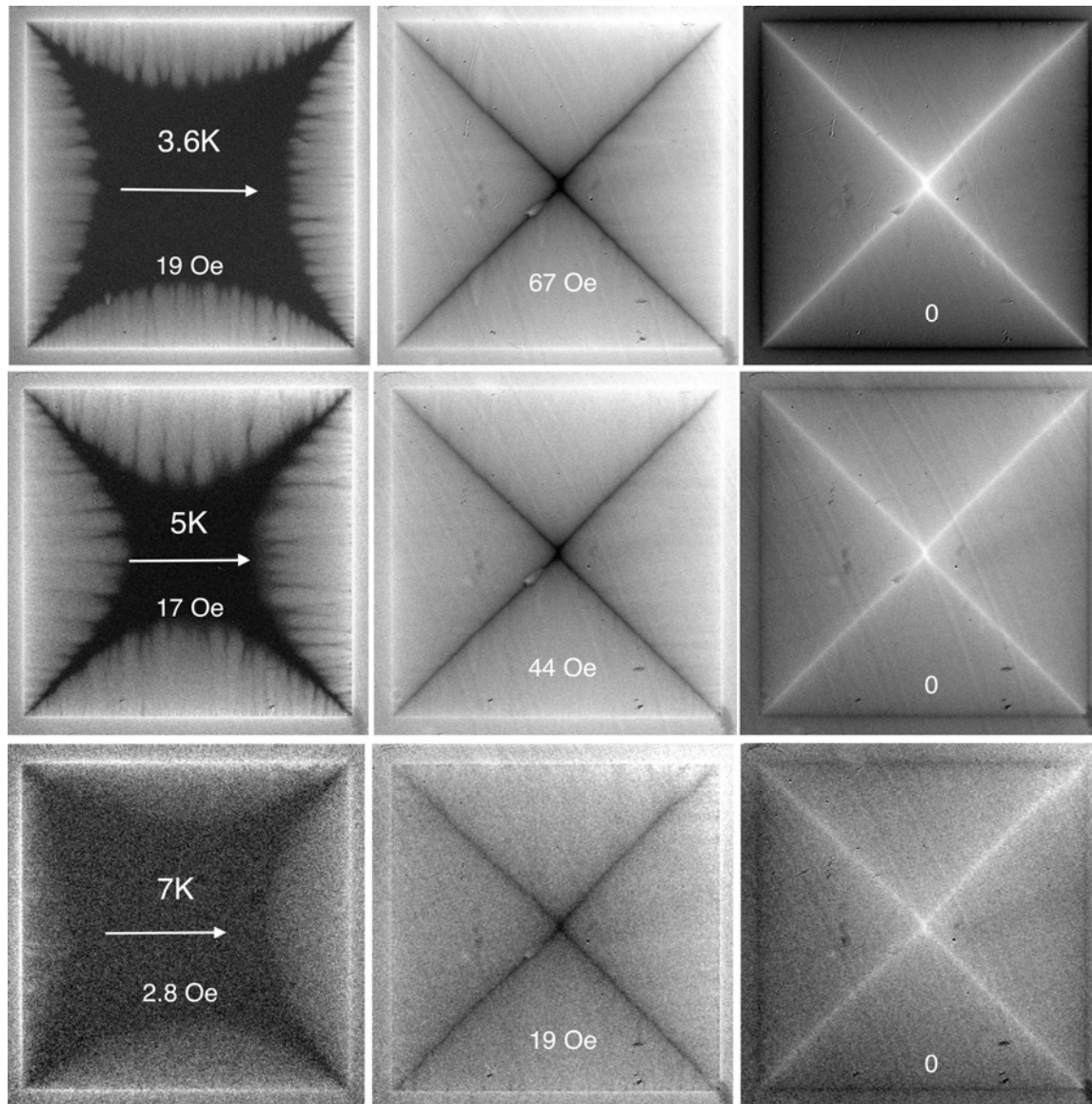
Fig.8 Normal flux patterns in 2x2mm square of 100nm Nb film at T=3.6, 5, and 7K. First and second columns illustrate $B_\perp$ distribution at increasing $H_\perp$ and the third column shows $B_\perp$ patterns at decreasing $H_\perp$. The in-plane field of 965 Oe practically yields no effect on the normal flux entry.
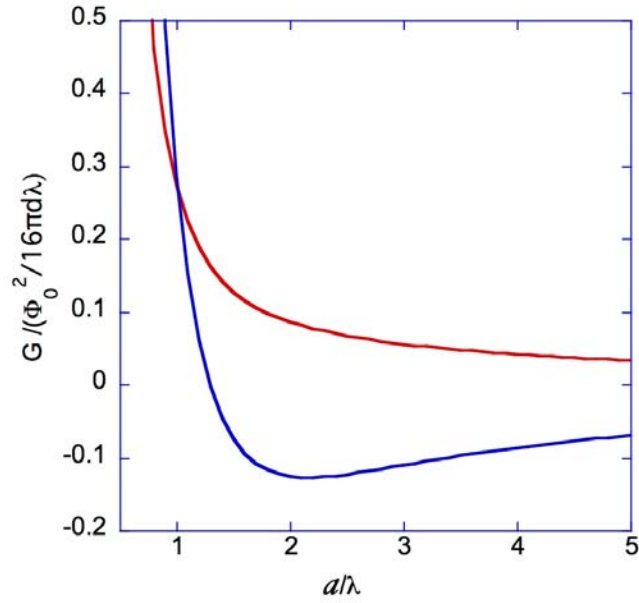
Fig.9 Gibbs potential, G, for in-plane vortices as a function of the inter-vortex distance, *a,* for a single vortex row in 100nm and 200nm films at H$_{||}$=1 kOe. See details of the calculations in the text.
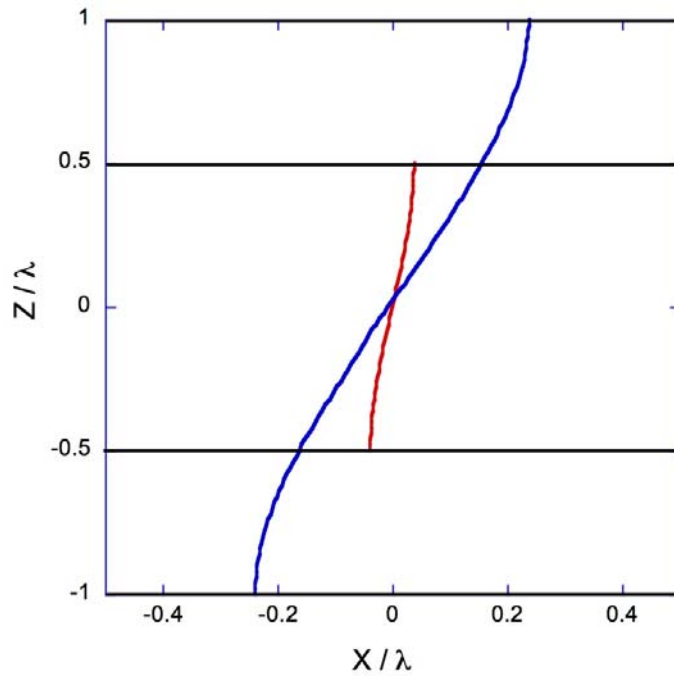

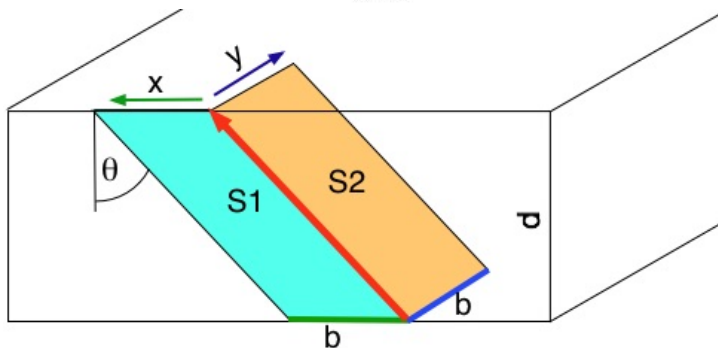Fig.10 Calculated shape of tilted vortices in 100nm and 200nm Nb films.

Fig.11 Cartoon of the areas swept by a tilted vortex (red arrow) moving by the same distance *b* along (s1) and across (s2) the tilt plane in the film of thickness *d*.